Materials Research Express

PAPER • OPEN ACCESS

Microstructure and mechanical properties of Fe-ZTA cermet prepared by vacuum hot-pressed sintering

To cite this article: Daming Sun *et al* 2020 *Mater. Res. Express* **7** 026518

Materials Research Express

OPEN ACCESS

RECEIVED
31 October 2019

REVISED
23 January 2020

ACCEPTED FOR PUBLICATION
28 January 2020

PUBLISHED
10 February 2020

PAPER

Microstructure and mechanical properties of Fe-ZTA cermet prepared by vacuum hot-pressed sintering

Daming Sun[1,2], **Xiaosong Jiang**[1,2], **Hongliang Sun**[1,2], **Tingfeng Song**[3] and **Zhiping Luo**[4]

[1] Key Laboratory of Advanced Technologies of Materials, Ministry of Education, Chengdu 610031, People's Republic of China
[2] School of Materials Science and Engineering, Southwest Jiaotong University, Chengdu Sichuan 610031, People's Republic of China
[3] Institut de Ciència de Materials de Barcelona (ICMAB-CSIC), Campus UAB, Bellaterra 08193, Barcelona, Spain
[4] Department of Chemistry and Physics, Fayetteville State University, Fayetteville, NC 28301, United States of America

E-mail: xsjiang@swjtu.edu.cn

Keywords: ZTA, vacuum hot-pressed sintering, cermet, interface bonding, grinding ratio, surface roughness

Abstract

The cermet based on metallic iron with zirconia toughened alumina (ZTA) as the reinforcing phase was prepared by vacuum hot-pressed sintering. The ZTA particles were subjected to electroless nickel plating to improve the interfacial bonding ability of ZTA and Fe matrix. In this paper, after electroless nickel plating, the effects of different particle sizes and different contents of ZTA particles on the grinding properties of Fe-based ZTA (Fe-ZTA) cermets were investigated. The results show that the ZTA particles are tightly bound to the Fe matrix. An interface layer is formed between the ZTA particles and the Fe matrix and it can improve the grinding ability of the Fe-ZTA cermet. By reducing the particle size and the content of ZTA particles, the friction coefficient between Fe-based ZTA cermet and the machined surface can be increased, and the surface roughness of the machined surface will reduce. When the ZTA particle size is F14 and the iron binder content is 40%, the friction coefficient between the Fe-ZTA cermet and the steel bar is 0.4981, the surface roughness of steel bar is 40.164 μm, the grinding ratio is 685.952.

1. Introduction

Due to the high hardness, high wear resistance and good fatigue performance, iron-based cermets have attracted more and more attention in the field of tool manufacturing and high wear resistance tools in recent years [1–3].The current research focus on how to use the reinforcement phase to improve the hardness and wear resistance of Fe-based cermets [3]. Ziejewska *et al* [4] found that the interface between the reinforcing phase and the matrix and the content of the reinforcing phase have an important influence on the grinding performance of the cermet. Therefore, a suitable reinforcement phase is the key to make cermets.

As a ceramic reinforcing phase, ZTA has been widely used in the field of making cermets. It was found in the study that the toughness of ZTA is greater than 12MPa $m^{1/2}$, which is several times than pure Al_2O_3 ceramics [5, 6].The ZrO_2 contained in ZTA undergoes a phase transition of t-ZrO_2 → m-ZrO_2 when subjected to stress, and compressive stress is generated at the crack tip during phase transformation, so that the crack closes under the tensile loading [7, 8]. Moreover, the coefficient of thermal expansion (CTE) of ZTA is closer to the iron matrix [9]. Therefore, ZTA is a good candidate for the preparation of cermets with high mechanical properties [10]. It is worth noting that the interface bonding ability between ceramic materials and metals is weak. The wetting behavior of ceramics on metal substrates is one of the key factors that determining the properties of cermet. Some studies have found that the contact angles of Fe/Al_2O_3 and Fe/ZrO_2 reach 140° and 116 °, respectively [11, 12].This shows that the interface bonding ability between Fe and the two ceramic materials is very poor. Therefore, it is necessary to modify ZTA particles by metal coating [13].

Electroless plating is widely used as a surface metal coating treatment method in the manufacture of cermets [13–16].The metal coating on the ceramic surface is mutually soluble or reacted with the matrix metal to obtain a mechanical bonding interface or a reaction bonding interface to achieve a wetting effect. Ru *et al* [16] found

Table 1. Properties of raw materials and cermet formulations (wt%).

	Binding agent	ZTA	FeS_2	Na_3AlF_6	TiH_2	$CaCO_3$	La	Cr	graphite	WC	remark
F10-1	35	50	2.5	2.5	3	2	0.5	1	1	2.5	
F10-2	40	45	2.5	2.5	3	2	0.5	1	1	2.5	
F10-3	35	50	2.5	2.5	3	2	0.5	1	1	2.5	nickel plating
F10-4	40	45	2.5	2.5	3	2	0.5	1	1	2.5	nickel plating
F14-4	40	45	2.5	2.5	3	2	0.5	1	1	2.5	nickel plating
F14 + 16-1	35	25/25	2.5	2.5	3	2	0.5	1	1	2.5	nickel plating

electroless plated Ni and Cr on the surface of ZTA, and Ni and Cr diffused into the iron matrix under high temperature conditions, forming a diffusion interface layer, which improved the wettability of ZTA and matrix. In the existing literature, most of the Fe-ZTA cermets are prepared by molten metal die forging process [2, 17, 18], and the prepared Fe-ZTA cermet is often used to prepare wear-resistant materials, but the molding rate is low. The preparation of Fe-ZTA cermet material by powder metallurgy can effectively solve the problem of low molding rate of cermet and can achieve densification [19–22].

In this paper, Fe-ZTA cermet materials were prepared by vacuum hot-pressed sintering, and electroless nickel plating can improve the bonding ability of ZTA and Fe matrix. The effects of electroless nickel-plated ZTA particles, different iron binders and different particle sizes of ZTA on the mechanical properties of Fe-ZTA cermets were investigated. The grinding mechanism of Fe-ZTA cermet was discussed based on the grinding test of Fe-ZTA cermet.

2. Materials and methods

2.1. Material preparation

In this paper, six kinds of iron-based ZTA ceramics with different binder contents and different ZTA particle sizes were prepared. ZTA has a particle size of 2.00 mm (F10, 'F' for fixing abrasives for abrasives. '10' for mesh number), 1.40 mm (F14), and 1.18 mm (F16), divided into nickel-plated and non-nickel-plated ZTA. The iron binder is a mixture of iron, cobalt, copper and stannum (75%Fe, 10%Co, 10Cu, 5%Sn). The iron-based ZTA cermet substrate is reinforced by FeS_2, Na_3AlF6, TiH_2, $CaCO_3$, Cr, La, graphite, WC, etc The specific parameters are shown in table 1.

To prevent the metal powder from being oxidized during the ball milling process, the ball milling process used herein is wet ball milling, ZTA particles, iron binder and other materials were added to a ball mill jar and ball milled on a planetary ball mill (WL-1) at a rate of 200 r/min for 2 h. The ball milling medium was t-butanol. The ball to powder ratio is 1:2. After ball milling, the slurry was then taken out and placed in a freeze dryer (FD-A-50) for freeze drying for 24 h. Then, the raw material was placed in a Φ55 mm graphite mold for vacuum hot-pressed sintering (VHP-HAS-25). The steps to prepare the specimens are as follows: The graphite mold was placed on the graphite substrate, then a graphite heel block was placed in the graphite mold, after that the powder was put and the spacer was separated by graphite paper, finally then it was placed in another graphite heel block. After the sintering was completed, the specimens could be taken out after demolding, so the graphite mold would not be crushed. The tolerance for graphite punch is 55 mm and the tolerance for die is inner diameter of 55 mm and an outer diameter of 120 mm.

The sintering temperature is 1000 °C, the sintering pressure is 12 MPa and the holding time is 120 min The sintering temperature is 1000 °C because the melting point of iron is 1538 °C, and other elements added in the collective such as Co, Cu will lower the melting point (T_m) of the composite powder. The sintering temperature of the composite powder is usually between 0.7–0.8 T_m, based on the results of pre-experiment so the sintering temperature was set at 1000 °C. The sintering pressure is 12 MPa, which not only ensures the compactness of the composite, but also ensures that this pressure will not damage the graphite mold. The holding time of 120 min ensures that some liquid phase exists in the sintering process to promote densification. Excessive holding time will lead to coarse grain and affect the mechanical properties of the material. After the specimen is cooled to room temperature, it is taken out for grinding test.

After pressing, the density of the Fe-ZTA cermet was 1.85 g cm^{-3} and the size was Φ55*10 mm. The cermet is very stable and has almost no change in density and size before and after sintering. Since the particle size of the metal powder used in the preparation of the cermet and the ZTA particle size are different, the particle size of the ZTA does not change during the sintering process, and the ZTA will emboss on the surface of the composite material to form a specimen of the raisin cake type, but in general, the ZTA will disperse evenly inside the specimen. Therefore, the composite material is also dense and uniform. The specimen processing flow is shown in figure 1.

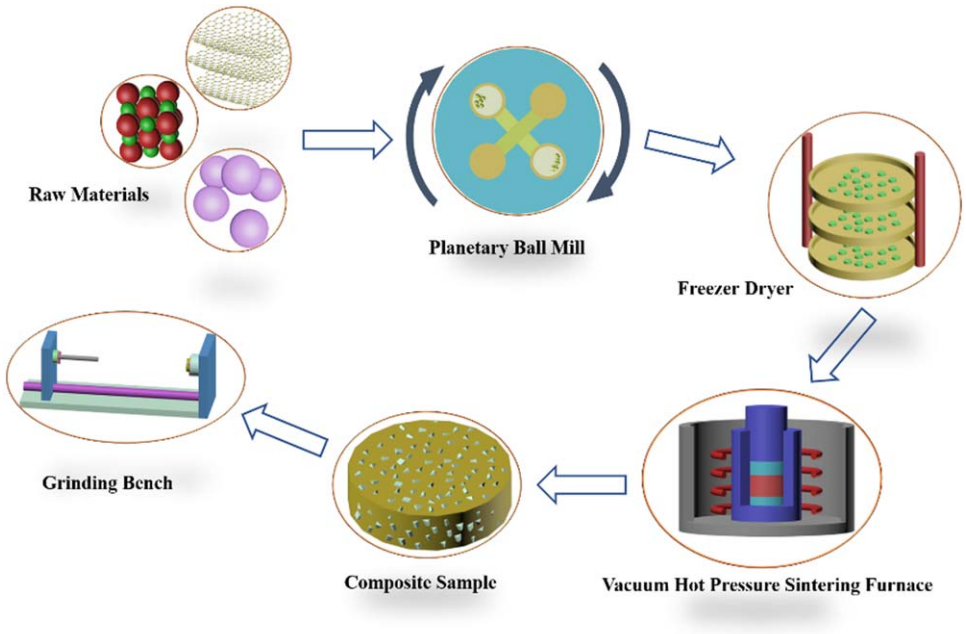

Figure 1. Flow chart of the Fe-ZTA cermet preparation.

Table 2. Chemical composition of the steel bars (wt%).

Steel grade	C	Si	Mn	S	P	V	Nb
U71Mn	0.65–0.76	0.15–0.35	1.10–1.40	⩽0.030	⩽0.030	⩽0.030	⩽0.010

In this paper only the particle size and content of ZTA particles and the effect of electroless nickel plating on the surface of ZTA particles on the properties of Fe-ZTA cermets were investigated. The input materials parameters (such as the content of graphite, WC, FeS_2, etc) in this paper have not been systematically studied. In the future research, the effect of input materials parameters on performance will be studied.

2.2. Characterization of the Fe-ZTA cermets

The microstructure of Fe-ZTA cermet was examined and analyzed by scanning electron microscopy (SEM, Hitachi S-4800) equipped with energy dispersive spectroscopy (EDS) and x-ray diffractometry (XRD, X. Pert Pro-MPD).The hardness of the composite was tested by digital microhardness tester (HVS-30).The friction coefficient of the surface between Fe-ZTA/steel bar interface and the surface roughness of steel bar were tested by self-made equipment. The grinding ratio of several cermets to steel bars was tested to characterize the grinding ability of Fe-ZTA cermets. The Fe-ZTA cermet is fixed on the rotor at a speed of 600 r/min and a grinding pressure of 500 N. The chemical composition of the steel bar is shown in table 2.After the grinding was completed, the surface wear morphology of the worn steel bar was analyzed by SEM and the grinding ratio of Fe-ZTA cermet was calculated.

3. Results and discussion

3.1. Electroless nickel plating of the ZTA particles

Figure 2 show SEM images of ZTA particles before and after electroless nickel plating. It can be seen from figure 2(a) that the surface of the ZTA particles is uneven and has many voids. These voids form closed pores during hot press sintering, which increases the porosity inside the material and reduces the mechanical properties of Fe-ZTA cermet. The EDS spectrum results show that there are no changes in the composition of points 1, 2, and 3. Most of the elements are Al, O, and Zr. It can be proved that the material is ZTA composed of ZrO_2 and Al_2O_3.

Figure 2(b) is an SEM image of the surface of ZTA particles after electroless nickel plating. It can be seen from figure 2(b) that the surface of the ZTA particles is uniformly covered with a layer of Ni, and the porosity is greatly reduced. The presence of the nickel plate layer also allows the ZTA to better contact the binder during the

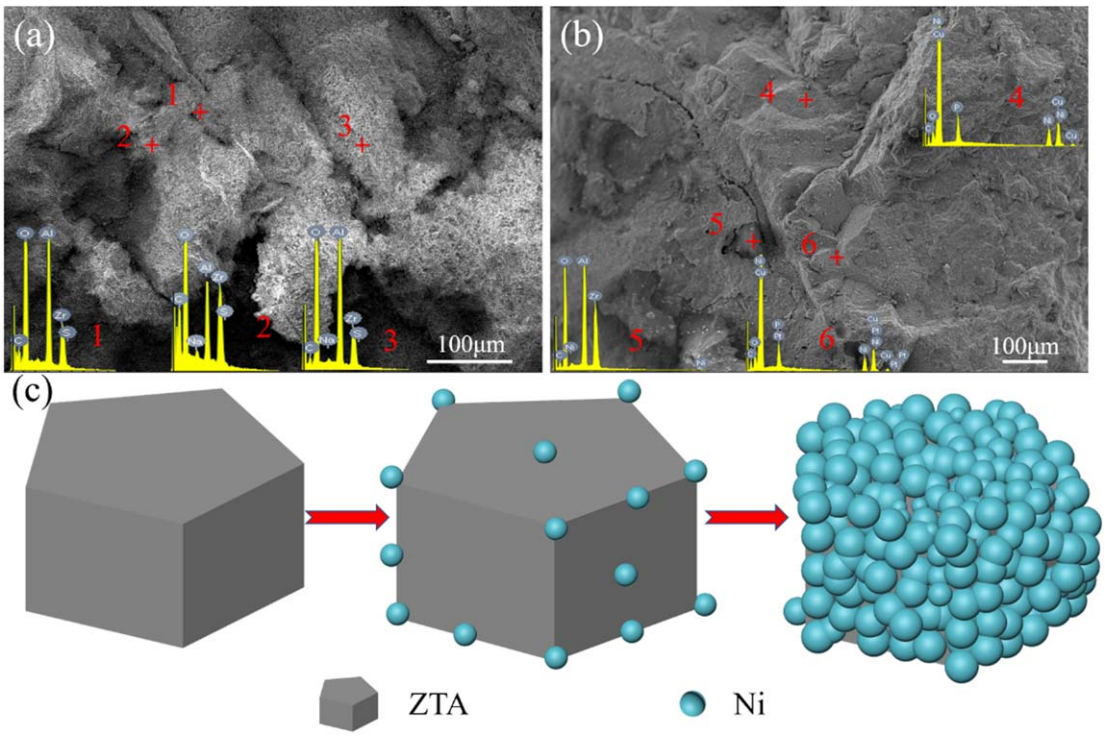

Figure 2. SEM images of ZTA particles (a) ZTA particles before electrolessly plated, (b) ZTA particles after electroless nickel plating, (c) Schematic diagram of surface electroless plating of ZTA particles.

sintering process, thereby improving the interface bonding ability [15]. The EDS spectrum results confirmed that ZTA was covered by the Ni layer at two points of 4 and 6. The nickel content at point 5 is almost zero, and the elemental contents of Al and Zr are consistent with points 1–3, so the Ni layer is broken at point 5.

Figure 2(c) is a schematic view of the surface electroless plating of ZTA particles, ZTA is sensitized and activated prior to electroless nickel plating. In the initial stage, the ZTA particle surface can form Ni active sites at these protrusions and boundaries because of the presence of more protrusions and boundaries [16]. Ni atoms can be adsorbed at these positions. Then, as the electroless plating progresses, the Ni atoms gradually grow and connect to each other, and finally uniformly coat the surface of the ZTA particles to form a complete Ni layer.

3.2. SEM images of the Fe-ZTA cermet

As six cermets were prepared by the same process, only the content and particle size of ZTA particles were changed, so the microstructure of the six Fe-ZTA cermets is the same. The microstructure of F14–4 specimens with the best tribological properties was studied, and the SEM images were shown in figures 3(a)–(f). It can be seen from figures 3(a) and (b) that there are four phases in the Fe matrix, and the reason is that the elements diffuse into the matrix during the sintering process. The EDS spectrum results show that the gray phase with the largest area is the Fe matrix, in which alloy elements such as Co are dissolved. The dark gray phase is a compound composed of Ti and O elements, and it is presumed that this phase is TiO_2. The white phase is mainly composed of Cu and Sn elements and is presumed to be Cu-Sn solid solution. The black flake phase is presumed to be graphite added to the raw material. Figures 3(c)–(f) are SEM images of the interface between ZTA and Fe. It can be seen from figures 3(c), (d) that ZTA is well bonded to the Fe matrix, and no pores are formed at the matrix, indicating that the matrix structure is tight and the interface layer exists in some regions. In figure 3(d), the Al_2O_3 and ZrO_2 on the ZTA side are layered, and ZrO_2 contained in ZTA is close to the iron matrix. In the enlarged view of figure 3(e), it can be seen that the stratification in ZTA more clearly. Figure 3(f) is an SEM image of the interface between ZTA and Fe matrix. Line scan result show that the interface is mainly composed of sulfides and carbides, it also contained a small amount of fluoride. The elements of Al, O and Zr are enriched on the ZTA side, the side of the substrate is mainly composed of Fe elements, and no diffusion of elements occurs on both sides.

3.3. XRD results of the Fe-ZTA cermets

XRD analysis was conducted on the specimens of F14–4, and the results were shown in figure 4. The XRD results in figure 4 show that some phase transitions occur in the Fe matrix, the matrix components are mainly γ-Fe and

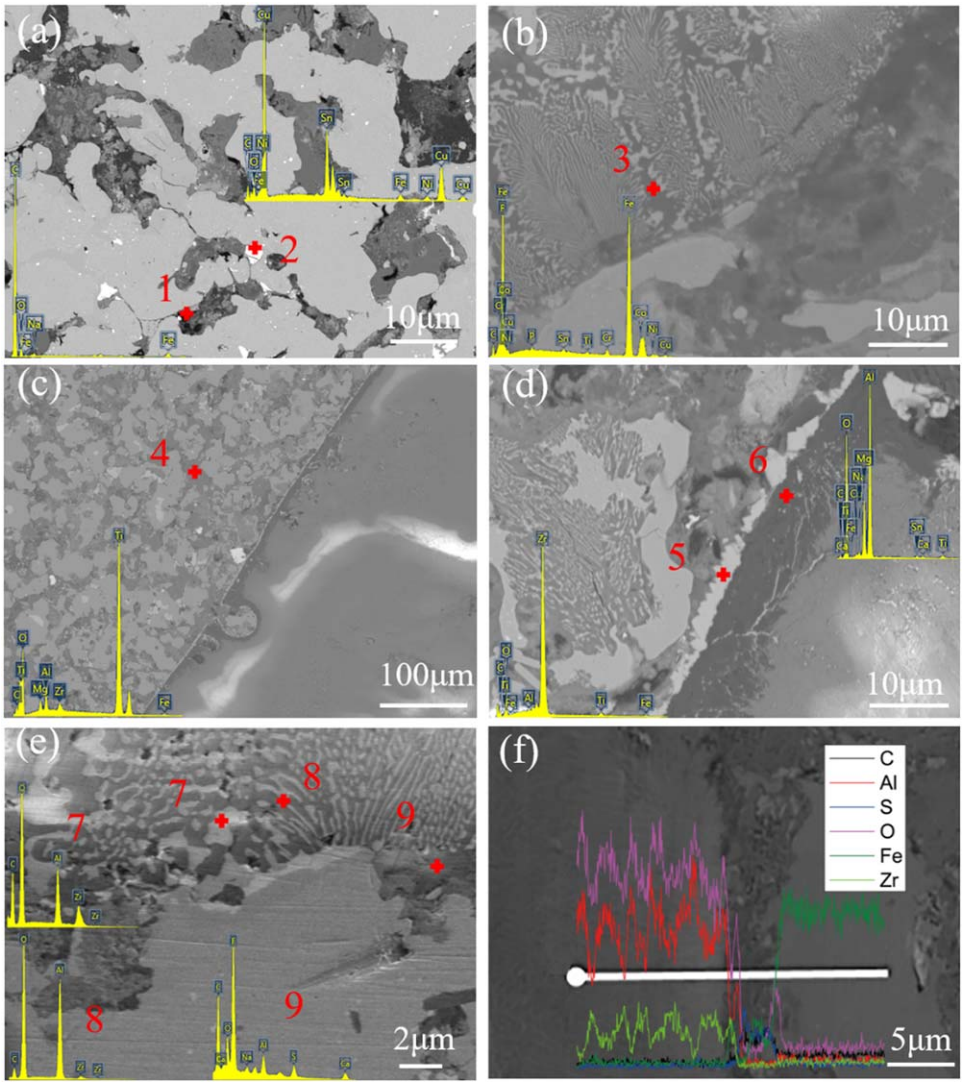

Figure 3. F14–4 Fe-ZTA cermet (a), (b) SEM images of Fe matrix, (c), (f) SEM images of ZTA/Fe interface.

$CoFe_{15.7}$ solid solutions. Since both Co and Fe are iron-based elements, Co atoms diffuse into the Fe matrix under high temperature and high pressure to form a $CoFe_{15.7}$ solid solution, and the hardness of the matrix is enhanced by solid solution strengthening. In figure 3(a), Cu and Sn form a solid solution, but the diffraction peaks of Cu and Sn disappear because their content is too small, lower than the threshold of XRD detection. The second phase component in the matrix is TiO_2. ZTA particles are composed of Al_2O_3 and ZrO_2, the m-ZrO_2 phase was found in the XRD results, which indicates that ZrO_2 has a phase transition from t-ZrO_2 → m-ZrO_2.The bulk expansion and shear strain during phase transformation can absorb the thermal stress and improve the toughness of Fe-ZTA cermets [9].

3.4. Surface scanning results of the Fe-ZTA cermets

The Fe/ZTA interface was analyzed by SEM equipped with EDS, and the results were shown in figures 5(a)–(i). Figure 5(a) shows the surface scanning results of the interface of Fe-based ZTA cermet. Several different phases as described in figure 3 can be seen in figure 5(a). Figures 5(b)–(d) shows that the main elements on the ZTA side are three elements of Al, O and Zr, and the Fe element does not diffuse into the ZTA side. The matrix contains the most Fe (figure 5(e)) and some alloying elements are solidified. The second phase in the matrix is mainly composed of Ti and O element, combine with the XRD results, it is proved that the second phase in the matrix is TiO_2. According to the surface scanning result, elements such as S, O, Na, and Ti are concentrated at the interface between ZTA and Fe. Figure 5(e) proves that the black phase in the matrix is graphite. No element of Ni was found at the interface because Ni diffused into the Fe matrix during sintering to form a solid solution [23]. In addition, due to the low content of Ni, no Ni was found in the surface scanning results of the substrate.

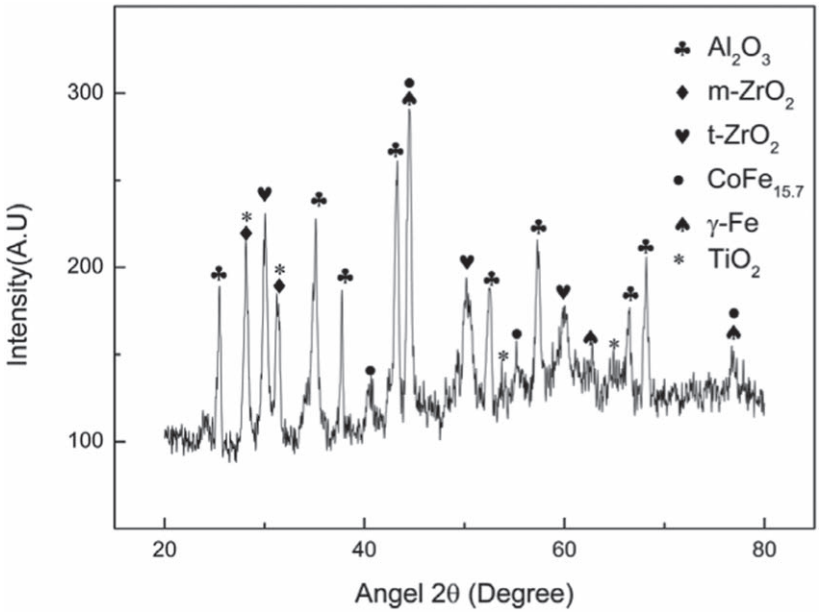

Figure 4. XRD pattern of specimen F14–4 Fe-ZTA cermet.

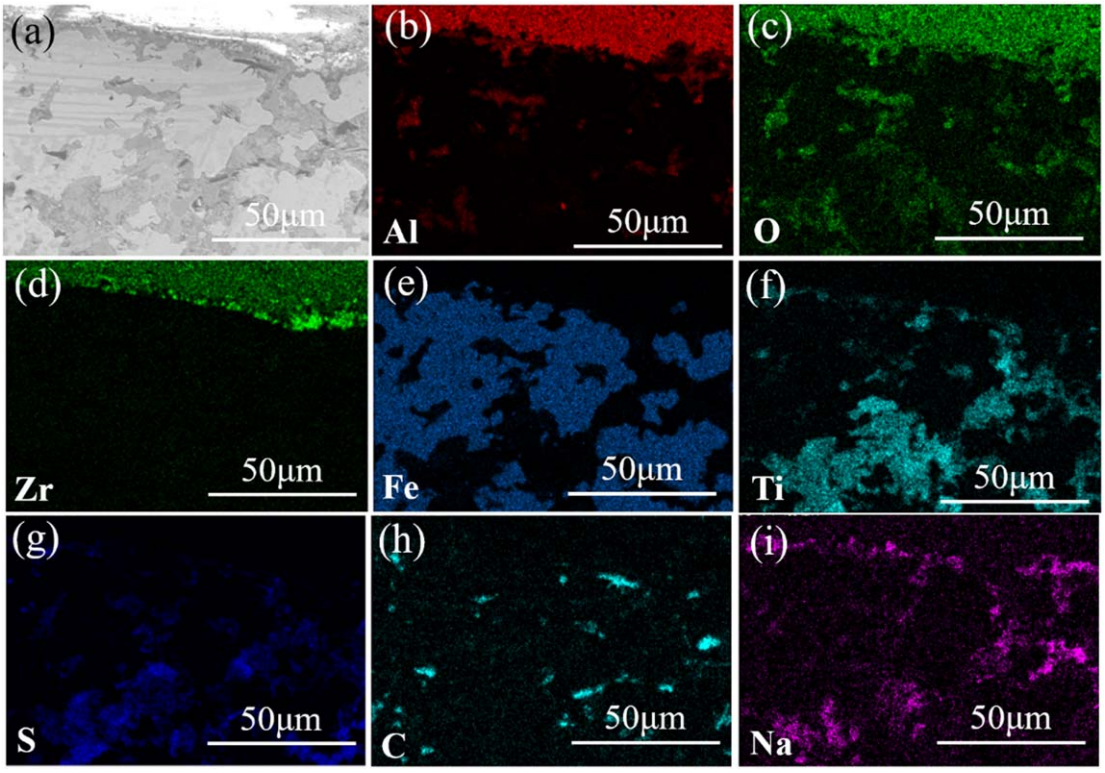

Figure 5. Surface scanning results of the Fe-ZTA cermets.

3.5. SEM image of the surface of the steel bar after grinding of four kinds of Fe-ZTA cermets

Figures 6(a)–(d) are SEM images and white light interferograms of the surface of the steel bar after grinding of Fe-ZTA cermets made of four kinds of electroless nickel-plated ZTA. The white light interferogram reflects the surface roughness Ra of the steel bar. In figures 6(a) and (b), there are some furrows and plastic deformation on the surface of the steel bar, and the surface of the steel bar is rough. The steel bar in figure 6(a) has a slight burning mark, indicating that a large amount of heat generated during the grinding process. When grinded by the Fe-ZTA cermet which contented low-diameter ZTA particles, the surface roughness of the steel bar decreases, furrow and plastic deformation disappear (figures 6(c), (d)). The white light diffraction pattern shows that the

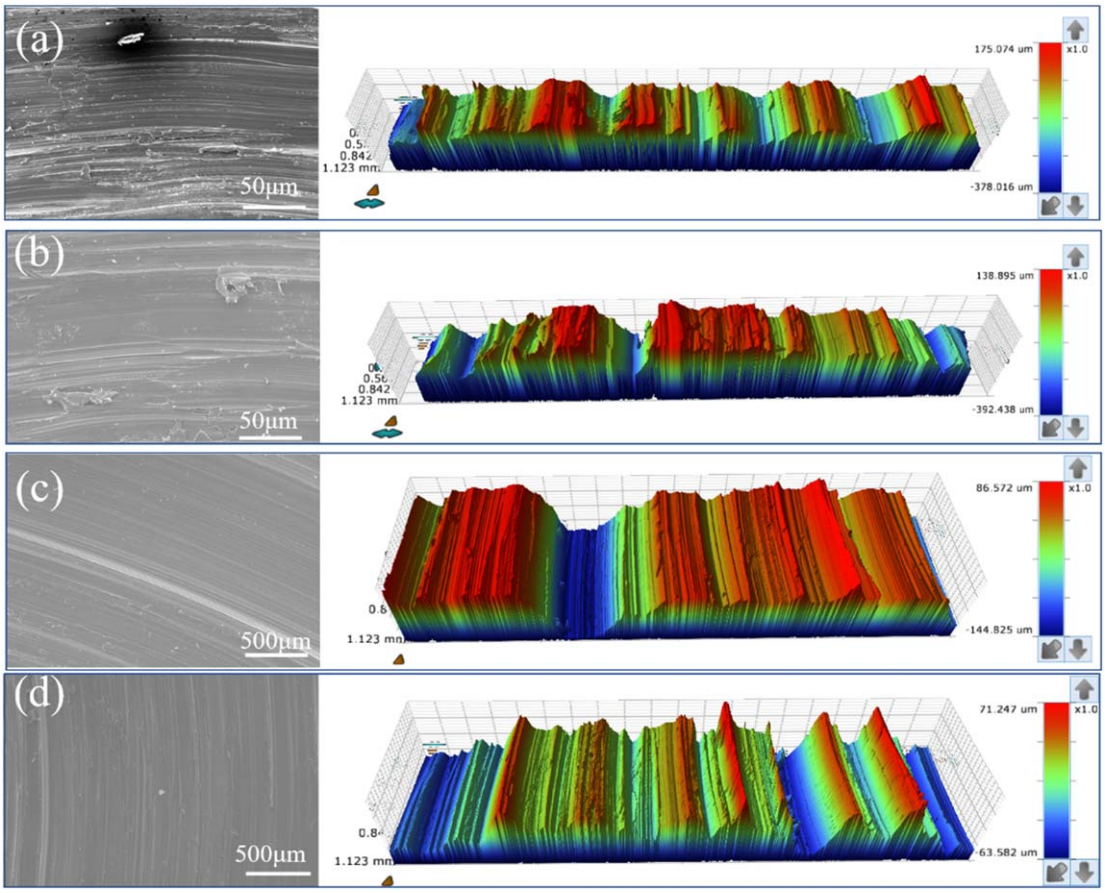

Figure 6. SEM and white light interferogram of the surface morphology of the steel bar after grinding (a) Using F10–3 Fe-ZTA cermet, (b) Using F10–4 cermet, (c) Using F14–4 Fe -ZTA cermet, (d) Using F14 + 16–3 Fe -ZTA cermet.

material surface is more uniform. The reason is that when the content of the binder is constant, the low-diameter ZTA particles can be better coated by the Fe matrix, some ZTA particles do not protrude from the surface of the cermet but uniformly distributed on the surface of the cermet. ZTA particles can be evenly contacted with the surface of the steel bar during processing, so the surface roughness of the steel bar is reduced [24].

3.6. Grinding test of the Fe-ZTA cermet

Friction coefficient of friction pair between Fe-ZTA cermet and steel bar changing with time was shown in figure 7(a). Figure 7(a) reflects the volatility of the friction coefficient. The smoother the friction coefficient curve, the better the grinding performance of this cermet. When the ZTA particle size is reduced, the friction coefficient curve is smooth, so that long-lasting effective grinding can be performed during the grinding process. The results of the friction coefficient between the six Fe-ZTA cermets and the steel bar are shown in figure 7(b). Comparing the specimens of F10–1, F10–2 and F10–3, F10–4 respectively, it can be found that the friction coefficient between the Fe-ZTA cermet and the steel bar reduced as the content of the binder increases. This is because when the content of the iron binder increases, the coating effect of the iron binder on ZTA increases, and the contact area between the ZTA and the surface of the steel bar is reduced, so the friction coefficient reduced. Comparing the F10–4, F14–4 and F10–3, F14 + 16–1 specimens, it can be found that when the particle size of the ZTA particles reduced, the friction coefficient of the friction pair increased, because the low-diameter ZTA particles can be more uniformly dispersed in the matrix, the contact area of ZTA to the matrix can be increased during grinding process, so the friction coefficient increased. Theoretically, the friction coefficient of Fe-ZTA cermets produced after electroless nickel plating should be higher [25]. However, the comparison of F10–1, F10–3 and F10–2, F10–4 specimens did not give a similar trend. Therefore, the effect of Fe-ZTA cermets made by electroless nickel plating on the surface roughness of steel bars and the grinding ratio of cermets was focused.

Figure 7(c) shows the surface roughness of the steel bars after grinding of the six cermets. Comparing the specimens of F10–1, F10–2, F10–3 and F10–4 respectively, it can be found that the surface roughness of the polished steel bar decreases with the increase of the iron binder content. The reason is that the increase of the iron binder content makes ZTA not easy to be exposed to the surface of the cermet, causing sliding friction

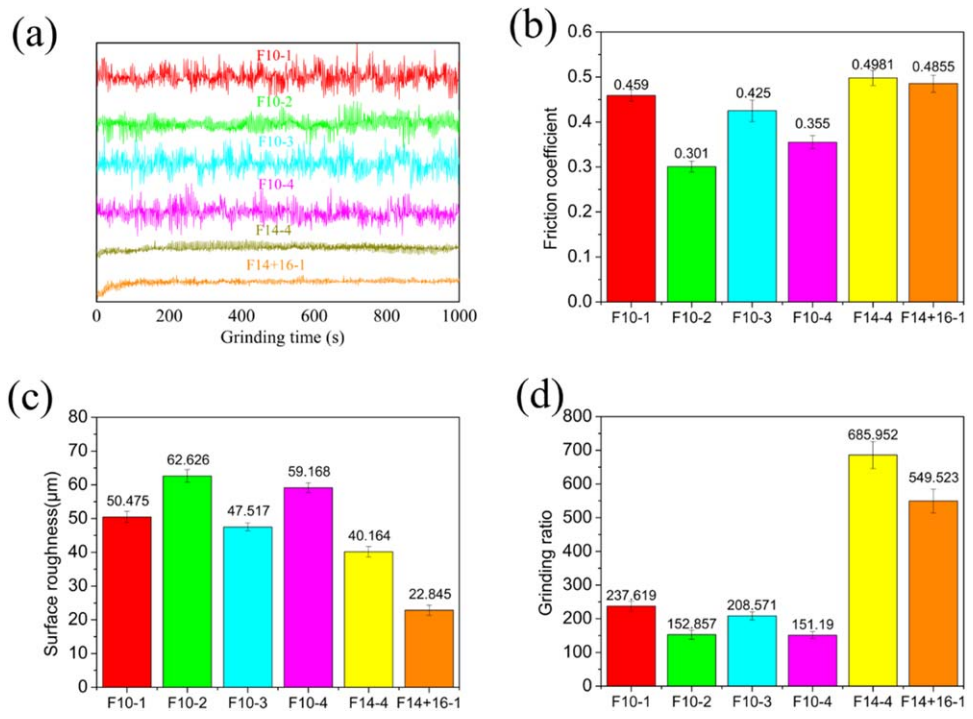

Figure 7. (a) Friction coefficient of friction pair between Fe-ZTA cermet and steel bar changes with time, (b) Friction coefficient of friction pair between Fe-ZTA cermet and steel bar, (c) Surface roughness of steel bar, (d) Grinding ratio of Fe-ZTA cermet.

between the steel bar and the metal substrate, which generates a large amount of heat to cause the surface burn of the steel bar (figure 6(a)). Comparing the F10–1, F10–3, F14 + 16–1 and F10–2, F10–4, F14–4 specimens, respectively, it was found that when the ZTA particle size is reduced, more ZTA particles can protrude from the cermet surface. Therefore, effective grinding can be produced to obtain a low surface roughness of the steel bar. Comparing the F10–1, F10–3, and F10–2, F10–4 specimens, when using Fe-ZTA cermet made of electroless nickel plated ZTA particles, the grinded steel bars have lower surface roughness. The specific reasons are described in section 3.7.

Figure 7(d) shows the grinding ratios of the six Fe-ZTA cermets. Comparing the specimens of F10–1, F10–2 and F10–3, F10–4, it can be found that the grinding ratio of the steel bar decreases as the content of the binder increases. The reason is that the increase in binder content is not conducive to the contact of ZTA particles with the steel bar. Therefore, the grinding amount and grinding ratios of the steel bar is reduced. Comparing the specimens of F10–1, F10–3, F14 + 16–1 and F10–2, F10–4, F14–4, respectively, it was found that when the ZTA particle size was reduced, the grinding ratio of the cermet produced by the low-diameter ZTA was 2–3 times than those cermets made of high-grain ZTA. The low-diameter ZTA can better exposure to the cermet surface to contact with the steel bar during the grinding process, so the grinding ratio increased. The effect of electroless nickel plating on the Fe-ZTA cermet grinding ratio is given in section 3.7.

3.7. Schematic diagram of cermet grinding on the surface of steel bars

Figure 8 is a schematic diagram of the grinding behavior of cermet. Firstly, the effect of electroless nickel plating on the grinding behavior of cermets was studied. Figure 8(a) is an initial state. As shown in figure 8(b), when grinding with F10–3 specimens, since the F10–3 specimen is made of electroless nickel-plated ZTA particles, ZTA is strongly bonded to the metal matrix during the grinding process and not easily peeled off from the iron matrix. As the grinding process proceeds, the ZTA particles are gradually broken. Finally, the protruding ZTA particles gradually wear to be parallel to the substrate. As the grinding process proceeds, the new ZTA abrasive grains are exposed to the surface of Fe-ZTA cermet. In figure 8(c), when using the F10–1 specimen for grinding, the ZTA particles have poor adhesion to the Fe matrix due to the absence of electroless nickel-plated ZTA particles. Under the condition of the tangential force during the grinding process, the ZTA particles will peel off from the substrate. The exfoliated ZTA particles will remain between the friction pairs, produce furrows and deep grinding grooves during the grinding process. The furrow and grinding groove increase the surface roughness of the steel bars. The sliding wear of the ZTA particles in the friction pair increases the wear quality of the steel bars and increases the grinding ratio. This also proves the conclusion of section 3.4.

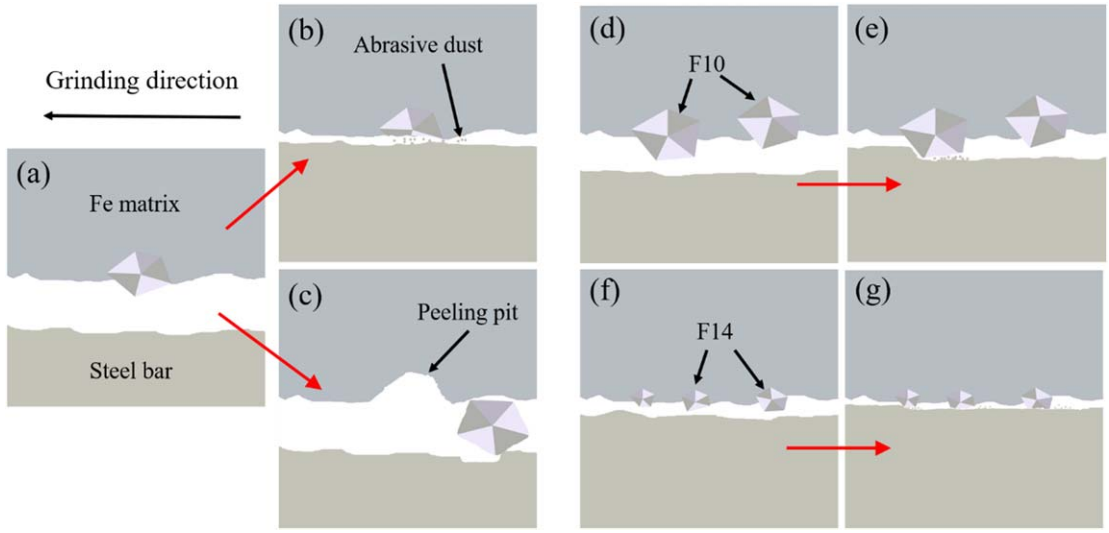

Figure 8. Schematic diagram of cermet grinding on the surface of steel bar. (a) Original state, (b) Wear behavior of specimen F10–3, (c) Wear behavior of specimen F10–1, (d) Original state of specimenF10–4, (e) Wear behavior of specimen F10–4, (f) Original state of specimen of F14–4, (g) Wear behavior of specimen F14–4.

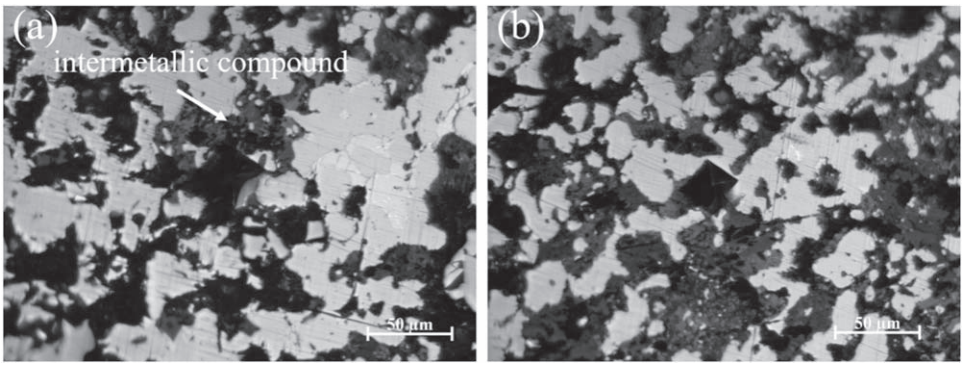

Figure 9. Micro Vickers hardness tester indentation. (a) On the intermetallic compound, (b) On the iron substrate.

When the particle size of ZTA changed, the schematic diagram of the grinding behavior of cermets on steel bars is shown in figures 8(d)–(g). When using F10 ZTA particles, the schematic diagrams are shown in figures 8(d)–(e).Use larger particle size ZTA particles, the ZTA particles protruding from the cermet surface will not be on the same level (figure 8(d)). During the grinding process, the prominent ZTA particles are in contact with the surface of the steel bar and gradually wear and consume until it is parallel with other ZTA particles. This method of grinding has two disadvantages:(1) The initial ZTA particles will produce a deeper grinding groove during the grinding process, and the grinding groove is difficult to be covered during the subsequent grinding process, resulting in a decrease of the surface roughness;(2) Within the same time, this grinding method is inefficient, resulting in a lower grinding ratio of the Fe-ZTA cermet. When using F14 ZTA particles, the schematic diagrams are shown in figures 8(f)–(g). Due to the small particle size of ZTA, it can be evenly distributed on the surface of cermets. Therefore, each ZTA particle is in contact with the surface of the steel bar at the same time during the grinding process, so the surface roughness of the machined surface decreased. The amount of grinding of the steel bar is increased, and the grinding ratio of the produced cermet is increased.

3.8. Hardness of the Fe-ZTA cermet

Due to the same production process, the six Fe-ZTA cermets prepared in this paper have the same structure and no significant difference in hardness. Figure 9 shows the metallographic diagram of F14–4 specimens. The micro vickers hardness of Fe-ZTA cermet was tested and the indentation are shown in figure 9. Five hardness tests were performed on each specimen, and the mean hardness value was 162.7($\pm$7.6) $HV_{0.1}$. Compared with pure iron, the hardness of Fe-ZTA is greatly improved. The reason is that the iron binder is added with alloy elements such as Co, which will form a solid solution in the hot-pressed process. In addition, the addition of graphite and

$CaCO_3$ can also improve the hardness of the matrix. The hardness measured by indentation at the second phase (intermetallic compound) was 117.5(±6.1) $HV_{0.1}$, which was lower than that of the matrix. These low-hardness second phases are more prone to fracture in the grinding process, so that ZTA particles can be precipitated out of the friction pair in time, avoiding deep scratches on the processed surface, thus improving the quality of the processed surface [26].

4. Conclusion

1. Ni-modified ZTA particles were prepared by electroless plating. The compact Fe-ZTA cermets were prepared by vacuum hot-pressed pressing. The Ni layer on the surface of the ZTA particles diffuses into the matrix during hot pressing, while the Fe atoms replace the Ni atoms to form a tight ZTA/Fe interface.
2. During the sintering process, elements such as Co in the iron binder diffuse into the Fe matrix to form a $CoFe_{15.7}$ solid solution, which strengthens the matrix. The micro Vickers hardness of the substrate was 162.7 (± 7.6) $HV_{0.1}$, and the hardness was remarkably improved. The second phase component in the matrix is mainly TiO_2, and the hardness of the second phase is 117.5 (±6.1) $HV_{0.1}$.
3. The effects of binder content, electroless nickel plating and ZTA particle size on the grinding behavior of the fabricated Fe-ZTA cermet were analyzed. Grinding test results show that Fe-ZTA cermet made of electroless nickel-plated ZTA can reduce the surface roughness of the machined surface and the friction coefficient of the friction pair, but slightly reduce the grinding ratio of the cermet; When the content of the iron binder increases, the surface roughness of the steel bar increases, the grinding ratio and the friction coefficient of the friction pair decreases; When using low-diameter ZTA particles, the cermet grinding ratio produced 2–3 times higher than that of the high-diameter cermet. At the same time, the friction coefficient of the friction pair is increased, and the surface roughness of the steel bar after processing lowered. F14–4 specimen has the best grinding performance, the grinding ratio was 685.952, the surface roughness Ra of the steel bar after processing was 40.164 μm, and the friction coefficient of the friction pair was 0.4981.

Acknowledgments

This work was supported by National Natural Science Foundation of China (No. 51201143), China Postdoctoral Science Foundation (No. 2015M570794, No. 2018T110993).

ORCID iDs

Daming Sun https://orcid.org/0000-0002-4469-1187
Xiaosong Jiang https://orcid.org/0000-0002-6703-9116

References

[1] Gu K K, Lin Q, Wang W J, Wang H Y, Guo J, Liu Q Y and Zhu M H 2015 Analysis on the effects of rotational speed of grinding stone on removal behavior of rail material *Wear* **342-343** 52–9
[2] Tang S L, Gao Y M and Li Y F 2014 Recent developments in fabrication of ceramic particle reinforced iron matrix wear resistant surface composite using infiltration casting technology *Ironmak. Steelmak.* **41** 633–40
[3] Fernandes C M, Willinger M G, Vieira M T and Senos A M R 2012 Interface exploring of tungsten carbide-stainless steel composites through HRTEM *Microsc. Microanal.* **18** 109–10
[4] Ziejewska C, Marczyk J, Szewczyk-Nykiel A, Nykiel M and Hebda M 2019 Influence of size and volume share of WC particles on the properties of sintered metal matrix composites *Adv. Powder Technol.* **30** 835-842
[5] WangJ S R 1989 Zirconia-toughened alumina (ZTA) ceramics *J. Mater. Sci.* **24** 3421–40
[6] Pfeifer S, Demirci P, Duran R, Stolpmann H, Renfftlen A, Nemrava S, Niewa R, Claub B and Buchmeiser M R 2016 Synthesis of zirconia toughened alumina(ZTA) fibers for high performance materials *J. Eur. Ceram. Soc.* **36** 725–31
[7] Basu B 2005 Toughening of yttria-stabilised tetragonal zirconia ceramics *Int. Mater. Rev.* **50** 239–56
[8] Mamivand M, Asle Z M and El K H 2014 Phase field modeling of stress-induced tetragonal-to-monoclinic transformation in zirconia and its effect on transformation toughening *Acta Mater.* **64** 208–19
[9] Sui Y, Zhou M and Jiang Y 2018 Characterization of interfacial layer of ZTA ceramic particles reinforced iron matrix composites *J. Alloy. Comp.* **741** 1169–1174
[10] Zhao H W, Li J H, Guo S B, Fan D D, Liu G H and Li J T 2017 Fast preparation of ZTA-TiC-FeCrNi cermets by high-gravity combustion synthesis *Ceram. Int.* **43** 6904–6909
[11] Eberhart J and Mcdonald J 1965 Adhesion in aluminum oxide-metalsystems *Trans. Metall. Soc. AIME.* **233** 512–517
[12] Munoz M C, Gallego S, Beltrán J I and Cerda J 2006 Adhesion at metal-ZrO_2 interfaces *Surf. Sci. Rep.* **61** 303–344
[13] Ru J J, Jia Y, Jiang Y, Feng J, Zhou R, Hua Y and Wang D 2016 Modification of ZTA particles with Ni coating by electroless deposition *Surf. Eng.* **33** 353-361

[14] Ru J J, He H, Jiang Y H and Zhou R 2019 Wettability and interaction mechanism for Ni-modified ZTA particles reinforced iron matrix composites *J. Alloy. Compd.* **786** 321–329
[15] Fan L, Wang Q, Yang P, Chen H H, Hong H P, Zhang W T and Ren J 2018 Preparation of nickel coating on ZTA particles by electroless plating *Ceram. Int.* **44** 11013–11021
[16] Ru J J, He H, Jiang Y H, Zhou R and Hua Y X 2019 Ionic liquid-assisted preparation of Ni–Cr Dual wrappedzta particles for reinforced iron-based composites *Adv. Eng. Mater.* **21** 1801120
[17] Tang S L, Gao Y M, Li Y F and Zheng Q L 2016 Preparation and interface investigation of Fe/Al_2O_{3P} composite activated by Ni and Ti *Adv. Eng. Mater.* **18** 1913–1920
[18] Zhou M J, Sui Y D, Chong X Y and Jiang Y H 2018 Wear resistance mechanism of ZTA(p)/HCCIcomposites with a honeycomb structure *Metals-Basel.* **8** 1–13
[19] Ji W B, Zou B, Liu Y N, Huang C M and Guo P 2017 Frictional behavior and wear resistance performance of gradient cermet composite tool materials sliding against hard materials *Ceram. Int.* **43** 7816–7826
[20] Akhtar F, Askari S J, Shah J A and Guo S J 2007 WITHDRAWN: processing, microstructure and mechanical properties of TiC–465 stainless steel/465 stainless steel layer composites *J. Alloy. Compd.* **43** 9287–9293
[21] Li B H, Liu Y, Cao H, He L and Li J 2009 Rapid fabrication of *in situ* TiC particulates reinforced Fe-based composites by spark plasma sintering *Mater. Lett.* **63** 2010–2012
[22] Wu Y, Wang X, Long F, Shen Y F and Zou Z G 2009 Effect of C content on properties and microstructure of steel-bonded cemented carbide GT35 produced by *in situ* reduction of ilmenite *Mater. Sci. Forum* **546-549** 1633–1636
[23] Ru J J, Jiang Y H, Zhou R and Feng J 2017 Preparation of Ni-encapsulated ZTA particles as precursors to reinforce iron-based composites *Adv. Eng. Mater.* **19** 1700268
[24] Song D D, Wan L, Liu X P, Hu W D, Xie D L and Wang J S 2016 Effect of hot pressing temperature on microstructure, mechanical properties and grinding performance of vitrified-metal bond diamond wheels *Int. J. Refract. Met. H.* **54** 289–294
[25] Wang W J, Gu K K, Zhou K, Cai Z B, Guo J and Liu Q Y 2018 Influence of granularity of grinding stone on grinding force and material removal in the rail grinding process *P. I. Mech. Eng. J-J. Eng.* **233** 355–365
[26] Gao S, Kang R K, Dong Z G, Zhang B and Wang Z G 2016 Surface integrity and removal mechanism in grinding sapphire wafers with novel vitrified bond diamond plates *MATER. Manuf. Process.* **32** 121–126